SAND2017-5315J

High Fidelity Polycrystalline CdTe/CdS Heterostructures via Molecular Dynamics

Rodolfo Aguirre[1], Jose J. Chavez[2], Xiaowang Zhou[2] and David Zubia[1]
[1]The University of Texas at El Paso
El Paso, Texas 79968, U.S.A
[2]Sandia National Laboratories
Livermore, CA 94550, U.S.A

ABSTRACT

The structural characteristics of polycrystalline CdTe solar cells play an important role in determining their electronic performance. Understanding of the structure at the meso and atomic scale is difficult to achieve through experiments alone including advanced Atomic Probe Tomography and Transmission Electron Microscopy. Alternatively, molecular dynamics simulations of polycrystalline growth of CdTe/CdS heterostructures have been performed. First, CdS was deposited on an amorphous CdS substrate, forming a polycrystalline film. Subsequently, CdTe was deposited on top of the polycrystalline CdS film. Cross-sectional images show grain formation at early stages of the CdS growth. During CdTe deposition, the CdS structure remains almost unchanged. Concurrently, CdTe grain boundary motion was detected after the first 24.4 nanoseconds of CdTe deposition. With the elapse of time, this grain boundary pins along the CdS/CdTe interface, leaving only a small region of epitaxial growth. CdTe grains are larger than CdS grains in agreement with experimental observations in the literature. Crystal phase analysis shows that zinc blende structure dominates over the wurtzite structure inside both CdS and CdTe grains. Composition analysis shows Te and S diffusion to the CdS and CdTe films, respectively. These simulated results may stimulate new ideas for studying and improving CdTe solar cell efficiency.

INTRODUCTION

CdTe is an ideal material for the development of high efficiency solar cells due to its ideal band gap [1] and excellent absorption coefficient [2]. Its theoretical efficiency limit is ~30% [3] and the highest laboratory efficiency obtained up to date is 22.1% [4], thus giving ~8% room for improvement. Obtaining greater efficiency can be achieved by increasing the open-circuit voltage (Voc) to above 1 volt without compromising short-circuit current (Jsc) and fill factor (FF). Higher Voc can be obtained by doping the CdTe to values higher than 10^{15} cm^{-3} [5]. Intrinsic defects in the CdTe such as point defects, dislocations and grain boundaries have demonstrated to impact in the dopability of the CdTe [6, 7, 8]. Surprisingly, the highest efficiency CdTe solar cells are made out of polycrystalline material [9]. Therefore, there should be some defects that are detrimental for the overall performance of the solar cell and other defects that are beneficial. For example, recent studies show that Lomer dislocations exhibit midgap states that increase electron-hole pair recombination rates, thus decreasing the solar cell efficiency [10]. On the other hand, in a different study it was found that intragrain Shockley partial dislocations cores do not introduce midgap states but they induce band bending, thus encouraging greater separation of carriers and improving cell efficiency [7]. Thus, it is important to study the formation and evolution of these defects in detail. Experimental techniques to study the structure of these defects such as Transmission Electron Microscopy (TEM) and Atomic

Probe Tomography (APT) are expensive and time consuming. On the other hand, Molecular Dynamics (MD) offers an alternative technique to study these defects at the atomic scale. In this paper, we apply MD simulations to study the growth of polycrystalline CdTe/CdS heterostructures. Our results show highly similar morphology, including defects and crystal structures, to that found in literature experiments.

THEORY

MD is a simulation technique capable of studying the growth of atomic layers. In conjunction with visualization tools, MD simulations offer three-dimensional atomic species maps, structural maps and dislocation maps. It also provides time evolution information of atoms during growth allowing to have a detailed analysis of the formation of defects. The MD simulations in this work were run using the Large-Scale Atomic/Molecular Massively Parallel Simulator (LAMMPS) [11]. This simulator was installed in the Gordon and Stampede high performance computing servers run by the San Diego Supercomputer Center (SDSC) and the Texas Advanced Computing Center (TACC), respectively. A Stillinger-Weber potential [12, 13] was used to define interatomic forces. Polycrystalline growth of the CdTe/CdS layers was achieved by using an amorphous CdS substrate of about 10 Å thick. Next, CdS was deposited on top to a thickness of ~80 Å using stoichiometric vapor ratio. Subsequently, a CdTe layer was deposited on top of the resulting CdS polycrystalline layer to a thickness of ~90 Å. Periodic boundary conditions were used in the plane direction (X and Z axes). Deposition temperature and rate were ~1200 K and ~0.002 Å/ps, respectively. Atomistic visualization and structural map was performed using the Open Visualization Tool (OVITO) [14]. Elemental concentration profile was measured in order to study intermixing.

DISCUSSION

Atomic species map and structure map of the polycrystalline CdTe/CdS layers after growth are shown in Figure 1. Cd, Te and S atoms are color coded black, purple, and yellow, respectively in Figure 1(a). Crystalline structures associated with each atom are color coded green and red for zincblende (ZB) and wurtzite (WZ) structures in Figure 1(b). Atoms that were not determined to be either ZB or WZ are colored blue and labeled UD. Notice, that UD atoms are located mostly at the surface, grain boundaries and substrate. White lines in Figure 1(b) indicate the interface between CdS and CdTe.

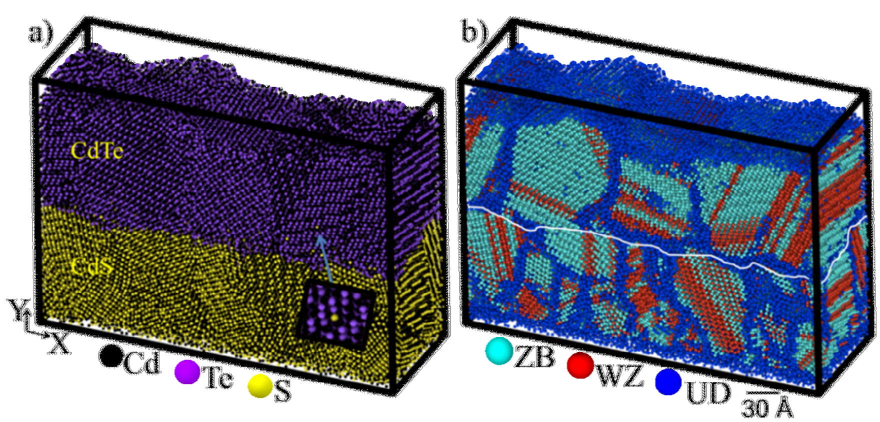

Figure 1: a) Atomic species map and b) structure map of the CdTe/CdS layers after growth.

Polycrystallinity of both the CdS and CdTe layer is observed as seen experimentally. Average grain size is smaller in CdS than in CdTe. Generally, the grains are detected as ZB structure for the most part. However, there is a general trend to detect thin WZ regions across the grains. On a closer look, these detected WZ regions are coherent twin boundaries, stacking faults or actual WZ phases. This is confirmed by looking at Figure 2 where a thin layer (5 Å) was sliced from the CdTe grown layer. Figure 2(a) shows the atomic species map and Figure 2(b) shows the structure map for this thin layer, respectively. Notice that the red atoms in Figure 2(b) correspond to the shaded areas in Figure 2(a). The red shaded areas are coherent twin boundaries, the green shaded area is a stacking fault and the yellow shaded is a WZ phase. Notice that the coherent twin boundaries and the stacking fault join in the vicinity of a Cd dangling bond error indicated by the green circle in Figure 2 (a). Also, notice that the stacking fault terminates also in a Cd dangling bond error as indicated by the black circle in Figure 2 (a) similar to those seen experimentally [7]. Moreover, a Te dangling bond error (red circle) is observed to provoke one of the stacking layers in the WZ phase in Figure 2 (a). Three-dimension animation across the sample at different positions in the X-direction reveals that these defects grow diagonally inside the grain starting at the CdTe/CdS interface and ending at the surface. However, there are other defects that extend across the grains without touching the interface or the surface. Defects in the CdS are seen to be of the similar type but shorter.

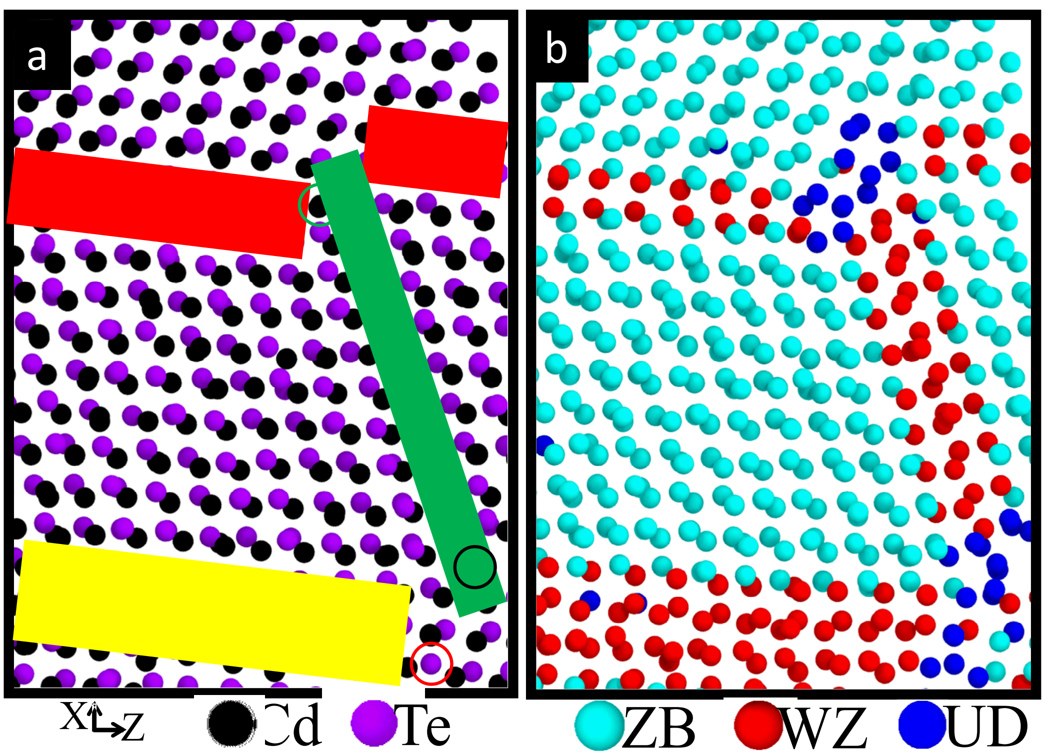

Figure 2: a) Atomic species map and b) structure map of a thin atomic layer sliced from the CdTe region.

On a different analysis, the initial stages of CdTe growth between 24.4 ns and 28.4 ns are shown in Figure 3. Grain boundary mobility was detected within these time frames. Before 24.4 ns, CdTe growth seemed to replicate the morphology of the CdS. However at 24.4 ns, a highly disorder region of large area starts to form as indicated by the yellow circle. At 25.2 ns, the atoms in the center of this large area had recrystallized by forming ZB and WZ structures resulting in the creation of a new grain. Between 26 ns and 27.6 ns the grain grows vastly. By 28.4 ns, the grain boundaries surrounding the new grain terminate right at the interface between the CdTe and CdS presumably to release strain due to lattice mismatch. Roughly, the velocity of the grain boundaries is 0.009 Å/ps which is 4× the magnitude of the growth rate of the film.

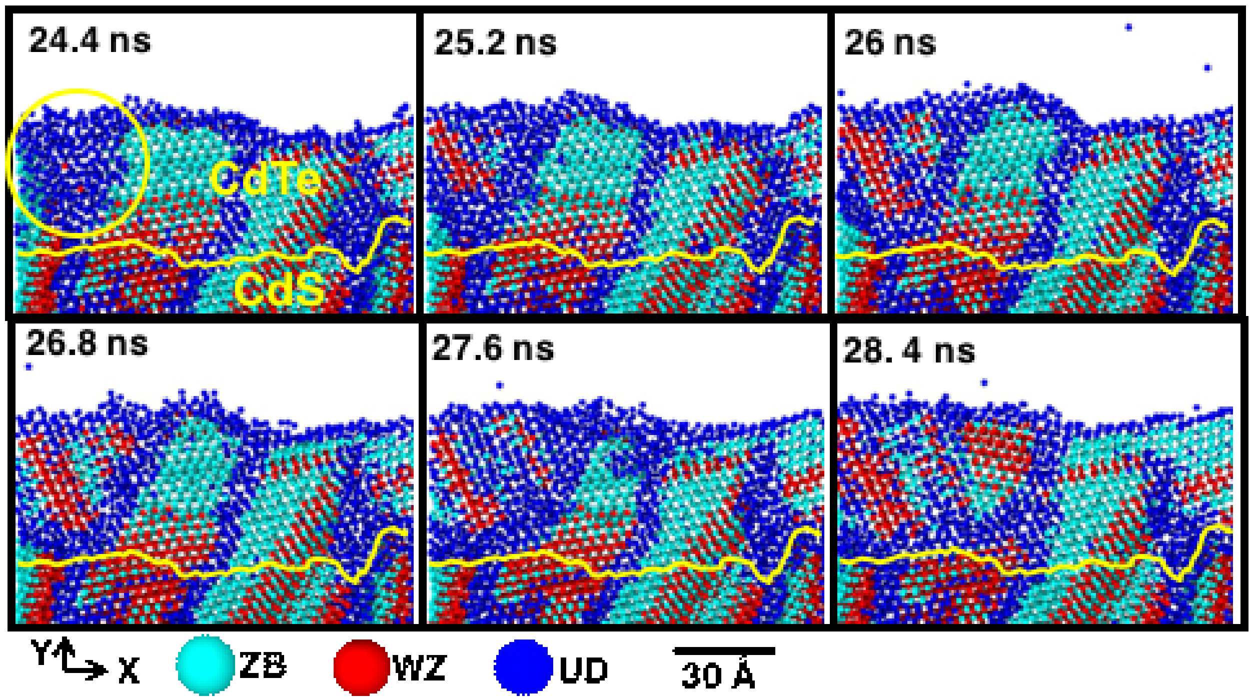

Figure 3: Initial stages of CdTe growth on CdS between 24.4 ns and 28.4 ns.

Intermixing and diffusion of the Cd and S atoms was also observed. This can be confirmed visually by looking at the S atom diffused to the CdTe layer and indicated by the magnified inset of Figure 1. No preferential diffusion trough grain boundaries was observed. Composition profile was generated and is presented in Figure 4. Notice that there is a highly symmetric diffusion profile of S and Te. Moreover, the volume density of CdTe is lower than the CdS as indicated by the step pointed by the black arrow in agreement with its increased lattice constant.

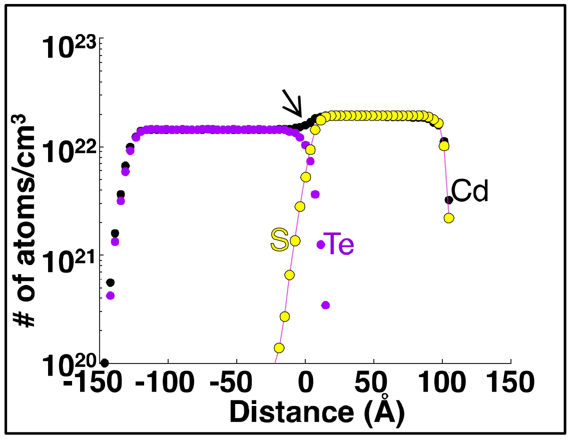

Figure 4: Composition profile of the CdTe/CdS after growth.

CONCLUSIONS

MD simulations were applied to reproduce the polycrystalline growth of CdTe/CdS heterostructure. Our predicted morphology is in good agreement with experimental observations. We show that the experimentally observed planar defects such as coherent twin boundaries and stacking faults can be reproduced with high fidelity. Some reproduced defects where found to grow diagonally across the grains starting at the CdTe/CdS interface and terminating at the CdTe surface, whereas other defects extend across grains but do not terminate at the CdTe/CdS interface or at the surface. Defects extending across the grains in the CdS layer are shorter due to smaller grains. Also, grain boundary migration was observed during the initial stages of CdTe growth presumably to mitigate the strain due to lattice mismatch in the interface. Grain boundary dynamics analysis indicates a grain boundary velocity of four times faster than the growth rate. Lastly, intermixing and diffusion between the CdTe and CdS interface was observed and did not show preferential diffusion through grain boundaries.

ACKNOWLEDGMENTS

This work was supported in part by the following grants: NSF/IGERT: DGE-0903670, DOE/BRIDGE:DE-EE0005958. Sandia National Laboratories is a multi-mission laboratory managed and operated by National Technology and Engineering Solutions of Sandia, LLC., a wholly owned subsidiary of Honeywell International, Inc., for the U.S. Department of Energy's National Nuclear Security Administration under contract DE-NA-0003525. This work used the computing resources provided by the Extreme Science and Engineering Discovery Environment (XSEDE) program, which is supported by National Science Foundation grant number ACI-1053575.

REFERENCES

[1] A. Balcioglu, R. K. Ahrenkiel, and F. Hasoon , J. Appl. Phys. 88, 12 (2000).

[2] R. W. Birkmire and E. Eser, Annu. Rev. Mater. Sci. 27 (1997).

[3] W. Shockley and H. J. Queisser, J. Appl. Phys. 32, 3 (1961).

[4] First solar press release, 2016. [Online].

[5] K. K. Chin, Sol. Energy Mater. Sol. Cells (2010).

[6] M. Tuteja, P. Koirala, S. MacLaren, R. Collins, and A. Rockett, Appl. Phys. Lett. 107, 142106 (2015).

[7] C. Li, Y. Wu, T. J. Pennycook, A. R. Lupini, D. N. Leonard, W. Yin, N. Paudel, M. Al-Jassim, Y. Yan, and S. J. Pennycook. Phys. Rev. Lett. 111, 096403 (2013).

[8] C. Li, Y. Wu, J. Poplawsky, T. J. Pennycook, N. Paudel, W. Yin, S. J. Haigh, M. P. Oxley, A. R. Lupini, M. Al-Jassim, S. J. Pennycook, and Y. Yan. Phys. Rev. Lett. 112, 156103 (2014).

[9] N. Strevel, L. Trippel, C. Kotarba, and I. Khan. Photovoltaics International, 22th edition.

[10] C. Sun, T. Paulauskas, F. G. Sen, G. Lian, J. Wang, C. Buurma, M. K. Y. Chan, R. F. Klie, and M. J. Kim. Scientific Reports, 6, 27009 (2016).

[11] S. Plimpton, J. Comp. Phys. 117, 1 (1995).

[12] F. H. Stillinger and T. A. Weber. Phys. Rev. B. 33, 1451 (1986).

[13] X. W. Zhou, D. K. Ward, J. E. Martin, F. B. van Swol, J. L. Cruz-Campa, and D. Zubia. Phys. Rev. B. 88, 085309 (2013).

[14] A. Stukowski, Modelling Simul. Mater. Sci. Eng. 18, 015012 (2010).